Technical Report

Background Suppression with Machine Learning in Volcano Muography

Gábor Galgóczi,[1,2] Gábor Albrecht,[1] Gergő Hamar,[1] and Dezső Varga[1]

[1]*HUN-REN Wigner Research Centre for Physics, Budapest 1121, Hungary*

[2]*Lorand Eotvos University, 1111 Budapest, Hungary*

Corresponding author: Gábor Galgóczi
Email address: gaborgalgoczi@gmail.com

Abstract

In this work, a machine learning algorithm, specifically a deep neural network, is introduced to mitigate background interference in muography applications, predominantly aimed at volcano imaging. The discussed detector system is engineered to filter out the low-energy background by incorporating up to five lead absorber layers interspersed among eight detectors. This detector system underwent a Monte-Carlo (Geant4) simulation to create training samples for the machine learning algorithm. It demonstrated that the devised deep neural network outperforms the traditional tracking algorithm in suppressing low-energy background, thereby rendering significant enhancement via machine learning supplementation.

Keywords: muography, machine learning, background suppression, Geant4, neural network
DOI: 10.31526/JAIS.2024.495

1. INTRODUCTION

Suppressing background in volcano muography is a critical task, given that the volumes of highest interest within volcanoes are situated not near the surface, but at a depth of around 1 km. A minuscule fraction (approximately 1%) of muons possess sufficient energy to traverse through 1 km of material. Nishiyama and colleagues demonstrated [1] that the background primarily comprises protons, electrons, and deflected muons. There is virtually no particle background above a kinetic energy of 1 GeV [1]. The penetrating muons, which constitute the signal, have at least a kinetic energy of 2–10 GeV, depending upon the thickness of the rock traversed. Thus, if a differentiation could be made between particles below 1 GeV and those above, the background could be almost entirely mitigated.

The degree to which muons scatter is heavily influenced by their energy. The probability density function (PDF) of scattering is described by the following approximation [2], which proposes roughly a Gaussian PDF:

$$\frac{dN}{d\alpha} = \frac{1}{\sqrt{2\pi}\alpha_{MS}} e^{-\frac{\alpha^2}{2\alpha_{MS}^2}}. \tag{1}$$

The PDF is symmetrical and it is centered around zero, having a standard deviation α_{MS}:

$$\alpha_{MS} = \frac{13.6\,\mathrm{MeV}}{\beta c p} Q \sqrt{\frac{x}{X_0}} \left(1 + 0.038 \ln\left(\frac{x}{X_0}\right)\right) \tag{2}$$

βc is the relativistic factor, x is the material thickness, p is the muon momentum, and Q is the charge number of the incident particle. α_{MS} also depends on the radiation length (X_0) which is empirically given by

$$X_0 \approx \frac{716.4 \frac{\mathrm{g}}{\mathrm{cm}^2}}{\rho} \frac{A}{Z(Z+1)\log\left(\frac{287}{\sqrt{Z}}\right)} \tag{3}$$

with Z and A being the atomic and mass numbers, respectively, and ρ is the material density.

Our team engineered the Muography Observation System (MOS), including approximately a total of 10 cm thick lead absorbers to suppress the background. This amount of material is sufficient to stop all electrons (which have a maximum 3 cm range per the continuous slowing down approximation for 500 MeV energy in lead). Regarding protons, the highest conceivable background energy is 1 GeV. The corresponding stopping power for these protons is 1.186 $\mathrm{MeV \cdot cm^2 \cdot g^{-1}}$.[1] Hence, they can penetrate 10 cm of

[1]NIST PSTAR: Stopping Power and Range Tables for Protons.

lead, retaining roughly 750 MeV of energy. Since their interaction predominantly occurs through ionization, akin to muons, they exhibit similar behavior. The primary distinction between protons and muons is their lesser relativistic nature due to their greater rest mass, causing increased scattering within the lead absorbers as per equation (2), mimicking the behavior of low-energy muons.

Numerous efforts are being made to comprehend and mitigate background particles. Rodriguez et al. [3] employed TOF (Time of Flight) to differentiate between various particles and muons across different energy spectra. Their findings indicate that the electromagnetic background has a median energy of 0.3 GeV, whereas muons have a median energy of about 3 GeV. Protons exhibit a flux that is two orders of magnitude lower than that of muons within the 1–100 GeV energy spectrum [1].

Our team developed and built a detector system called MOS [4, 5]. This system consists of 7–9 Multiwire Proportional Chambers (MWPCs) that register the trajectory of incoming particles. Each detector incorporates a set of wires aligned in one direction and a set of pads segmented perpendicularly in the other, thus cost-effectively recording the 1D projection of the particle's path in both directions. A mixture of argon and carbon dioxide gas is typically utilized within these detectors. Positioned between the MWPC detectors are lead absorbers, essential for suppressing background. The positions of the 9 detectors utilized in this work were the following measured from the first one: 120, 383, 644, 925, 1249, 1519, 1809, and 2072 mm. The positions of the lead absorbers from the same reference point were as follows: 503, 782, 1105, 1380, and 1660 mm.

More than ten detectors from our group have been operational on-site at the Sakurajima volcano, offering valuable insights into the volcano's activity [6]. Remarkably, the system documented the emergence of a volcanic plug beneath the Showa crater exclusively through muography [7].

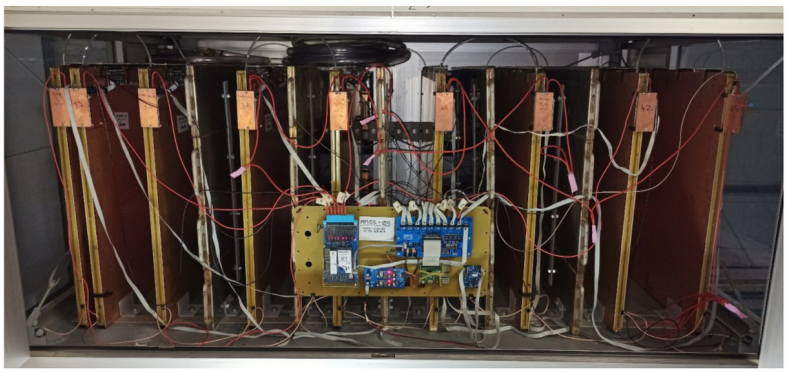

FIGURE 1: The MOS-09 system working at the Sakurajima volcano. 9 MWPC detectors and 5 lead absorbers are visible together with the readout electronics.

2. SIMULATION OF THE DETECTOR SYSTEM

The simulation of the detector system was carried out in Geant4 [8] (version 10.5). We utilized specific Geant4 classes, denoted as "Physicslists", to characterize the material interactions within. Among these, a preconstructed "General" physics list that contains all the physical processes to be considered by the simulation and two tailored lists for muons were used. This made it possible to investigate different settings for each relevant particle physics process in order to optimize for runtime. These muon-specific lists accounted for processes such as ionization, bremsstrahlung, pair production, multiple scattering, and capture. For the remaining particles, the defined electromagnetic interactions included the photoelectric effect, Compton scattering, pair production (for γ), ionization, and multiple scattering for electrons and positrons. The "General" physics list encompassed interactions and decays for hadrons and ions. The expected range at which secondary particles are generated within the simulation has a hard upper limit ("cut") of 0.1 mm.

A detailed detector geometry is considered in the simulation, including the electronic boards and the PCB copper layers. The detectors' gaseous volume, comprised of argon and carbon dioxide, was partitioned into cubic segments measuring $20 \times 12 \times 12\,\mathrm{mm}^3$. The simulation registered the energy deposition within these segments. Five lead absorbers, each 2 cm thick with lateral dimensions of 80 cm by 80 cm, were positioned after the second, third, fourth, fifth, and sixth detectors. These absorbers were encased in a steel cover with a thickness of 0.4 mm as illustrated in Figure 2. Muons were generated following an exponential energy distribution, ranging from 100 MeV to 1 TeV. The exponent was chosen to yield the same number of events below 5 GeV and above. This way the teaching sample for the binary classification was balanced. In order to cover the whole phase space for the potential direction of the incoming muons, the muons' point of origin was randomly selected on a sphere. Afterward, it was displaced in the plane perpendicular to the dimensions of the detectors. The individual wires were activated upon surpassing a 1 keV energy deposition threshold.

This simulation framework was used to generate training data for the machine learning model described in the following section, as well as validation data for the comparison between the ML and the tracking algorithm presented in the following sections.

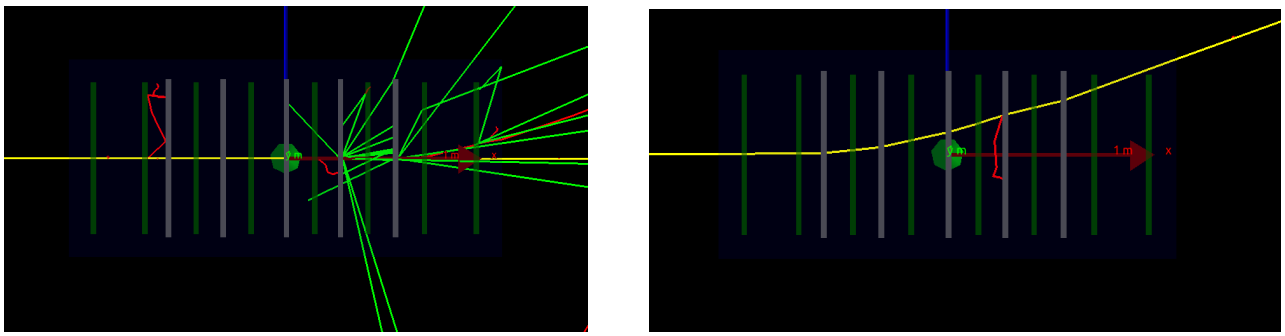

FIGURE 2: Two muons simulated in the MOS8-detector. On the left, a muon with 50 GeV initial energy crosses the detector without scattering and produces several γ-rays and electrons. On the right, a 500 MeV muon crosses the detector while scattering substantially. Yellow tracks are muons, red ones are electrons, blue ones are positrons, and green ones are γ-rays.

3. TRACKING ALGORITHM

This section describes a tracking algorithm routine that allows the identification of muons with low kinetic energy by applying a cut on the fit residuals. The tracking algorithm decouples the horizontal and vertical axes, denoted as X and Y, respectively. The tracking process starts with the clustering of hits. A straight line is fit to every possible permutation of the cluster centers. The sum of the reduced residuals (χ^2 value) is computed for each fitting, selecting the one with the smallest value. The spatial resolution of the detector, which is used for the reduced residuals, is calculated by leaving out one layer from the fit and then calculating the distance from the actual cluster center from the fit. This is only performed for tracks with a χ^2 value less than 2.

To enhance tracking efficiency, the algorithm can be configured to attempt fitting the straight line to cluster sets that encompass one or two clusters less than the number of chambers. For instance, in MOS-08, with 8 chambers and each wire having a triggering efficiency of around 95%, seeking muons that registered a cluster in all detectors would yield a tracking efficiency of 66%. However, aiming for at least one cluster in 7 detectors out of 8 boosts the tracking efficiency to approximately 95%. This is called the "N-1" setting. In the subsequent part of this paper, we utilized the latter tracking setting.

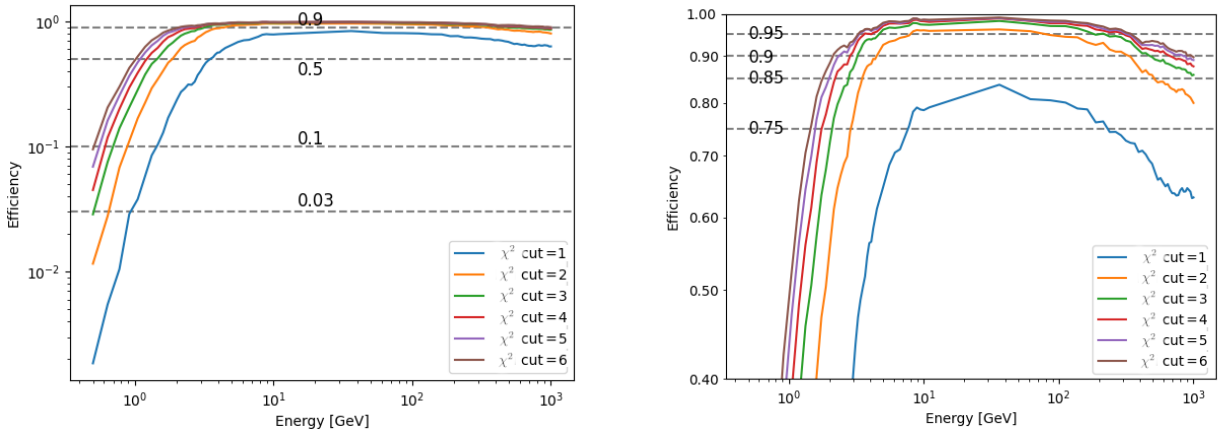

FIGURE 3: Efficiency (acceptance rate) of muons with different initial energies from Geant4 simulation for different χ^2 cuts. This plot focuses on background suppression. For example, a cut at 2 in χ^2 suppresses 80% of 1 GeV events.

A specialized simulation encompassing muons and the MOS-8 system was executed, with 20 million muons isotropically simulated from diverse directions. Only muons that would intersect the central half of the first and last detectors, assuming a straight path, were simulated. This was done to simulate only muons that have a cluster in all detectors. Events, with specified initial muon energy from the Geant4 simulation, were analyzed using the tracking algorithm to ascertain the proportion of muons detected relative to muon energy. Generally, muons below 1 GeV are deemed background in volcano muography and must be eliminated.

For particle tracking, it is important to introduce a cut in the χ^2 value to mitigate the presence of low- and medium-energy muons, which typically exhibit a high χ^2. Figure 3 showcases the efficiency of the tracking for varying cuts and distinct initial muon energies. A cut at 4 was employed in the subsequent work, aimed at optimizing the tracking efficiency, as this setting is the best compromise between high efficiency and a decent sub-GeV muon rejection. This algorithm with the "N-1" setting and with a χ^2 cut of 4 allows us to suppress 4% of the 0.5 GeV muons while maintaining a 99% efficiency at 15 GeV. In the next section, the performance of this algorithm will be compared to a DNN.

4. THE NEURAL NETWORK AND RESULTS ON ITS BACKGROUND SUPPRESSION

We opted for the utilization of Deep Neural Networks (DNNs) to decide whether the observed particle was of high-energy (signal) or of low-energy muon (background) as described in Section 1. Essentially, the machine learning algorithm was tasked with binary classification. TensorFlow version 2.11.0 was utilized for this purpose. The input data consists of all the hits (not clusters) in both directions (same format that was used for the tracking algorithm) and additionally the total energy deposition in each detector. The motivation for decoupling the different inputs helps the network since the hits in the X and Y directions are almost independent. This choice was tested experimentally; the decoupled subnetworks yielded a superior performance compared to a network that consists of fully connected layers. The outcomes from the subnetworks are concatenated, following which a fourth one classifies the event based on the passed features. The hyperparameters were optimized by hand, experimentally. 20 million events were fed into the network. Because of the similarity of the classification problem and the detector configuration with the NEWCUT experiment [9], we chose a similar DNN architecture:

(i) Rectified linear unit activation functions between each hidden layer

(ii) Sigmoid for the classification layer

(iii) 15 layers all together

(iv) 5000 neurons all together.

The dataset was split into training and validation data with a $9:1$ ratio. During fitting, the loss on the validation sample converged. No overfitting was observed. Figure 4. shows the efficiency of the neural network for 10000 simulated muons, which were independent of the validation and training events. This network outperforms the conventional χ^2 method by suppressing 1 GeV muons fourfold, as depicted in Figure 3. Moreover, unlike the classical algorithm, the efficiency for high-energy muons does not decrease. For instance, muons with an energy of 1 TeV exhibit an efficiency of 99.5% as opposed to 87% (with a χ^2 cut of 4). The reason behind the drop in efficiency of the tracking algorithm for high energy is the number of large clusters. Since the algorithm uses the center of the clusters if a large portion of the detector has hits, the χ^2 value can become large. We aim to investigate this effect further.

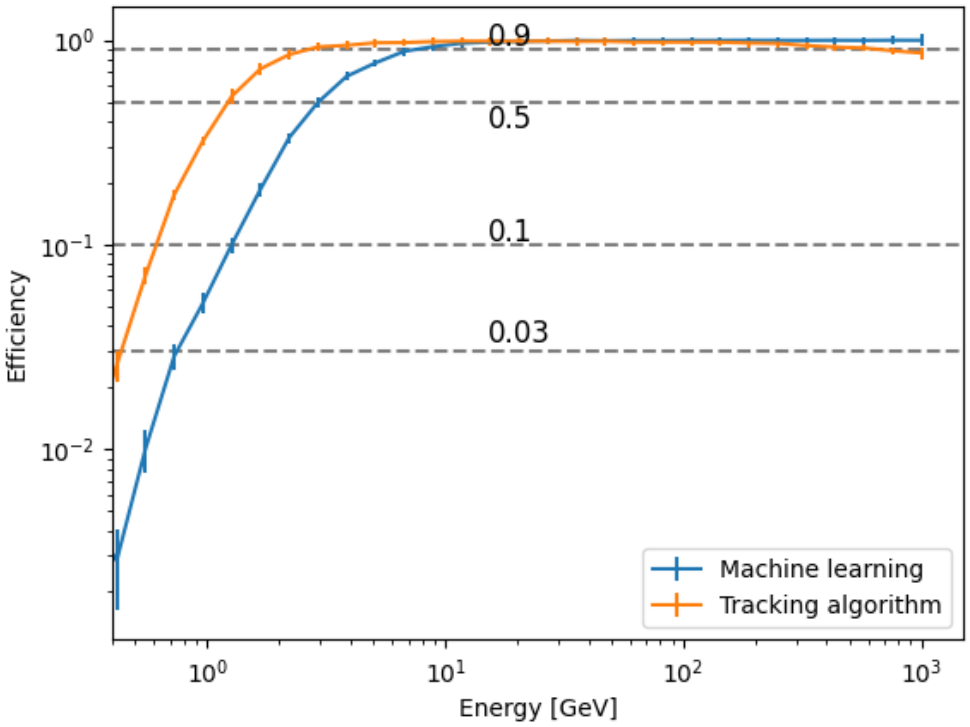

FIGURE 4: Efficiency (acceptance rate) of the simulated muons using the neural network with different initial energies.

5. CONCLUSION

In conclusion, the study detailed in this article showcases the novel application of machine learning in volcano muography for background suppression. The simulation data of the MOS detector system, equipped with multiple lead absorber layers, was used to train a deep neural network to distinguish between signal and background. The comparison between the traditional tracking algorithm and the neural network demonstrated a clear superiority of the latter in suppressing background interference while maintaining high efficiency for detecting high-energy muons. By suppressing the background four times better with the machine learning solution, we address the critical challenge of accurately imaging volcanic structures, particularly those situated at substantial depths.

CONFLICTS OF INTEREST

The authors declare that there are no conflicts of interest regarding the publication of this paper.

ACKNOWLEDGMENTS

This work was supported by the Joint Usage Research Project (JURP) of the University of Tokyo, ERI, with the project ID 2023-H-03. Additionally, support was garnered from the "INTENSE" H2020 MSCA RISE project, designated under Grant Agreement (GA) No. 822185, and the "Mine.io" HEU project, identified under GA No. 101091885. Financial backing was also provided by the Hungarian NKFIH research grant, allocated under ID OTKA-FK-135349 and TKP2021-NKTA-10. The János Bolyai Scholarship of the Hungarian Academy of Sciences further bolstered this work, alongside the ELKH-KT-SA-88/2021 grant. The construction and evaluation of detectors were carried out within the Vesztergombi Laboratory for High Energy Physics (VLAB) situated at Wigner RCP, ensuring a solid foundation for the research conducted.

References

[1] Nishiyama, R. et al., Monte Carlo simulation for background study of geophysical inspection with cosmic-ray muons. Geophysical Journal International 2606015 (2016). DOI: 10.1093/gji/ggw191.
[2] G. R. Lynch and O. I. Dahl, Approximations to multiple Coulomb scattering. Nucl. Instrum. Meth.B58, 6 (1991). DOI: 10.1016/0168-583X(91)95671-Y.
[3] Peña-Rodríguez, J. et al., Muography background sources: simulation, characterization, and machine-learning rejection. 37th International Cosmic Ray Conference proceedings (2021). DOI: 10.22323/1.395.0400.
[4] Varga, D. et al., High Efficiency Gaseous Tracking Detector for Cosmic Muon Radiography. Advances in high energy physics 1962317 (2016). DOI: 10.1155/2016/1962317.
[5] Varga, D. et al., Detector developments for high performance Muography applications. NIM A 162236 (2020). DOI: 10.1016/j.nima.2019.05.077.
[6] Oláh, L. et al., Investigation of the limits of high-definition muography for observation of Mt Sakurajima. Philosophical transactions of the Royal Society A 2018.0135 (2018). DOI: 10.1098/rsta.2018.0135.
[7] Oláh, L. et al., Plug Formation Imaged Beneath the Active Craters of Sakurajima Volcano With Muography. Geophysical research letters 10.1029 (2019). DOI: 10.1029/2019GL084784.
[8] Allison, J. et al., Recent developments in Geant4 Nuclear Instruments and Methods in Physics Research Section A: Accelerators, Spectrometers, Detectors and Associated Equipment, vol. 835, 186–225 (2016). DOI: 10.1016/j.nima.2016.06.12.
[9] Olah, L. et al., Development of Machine Learning-Assisted Spectra Analyzer for the NEWCUT Muon Spectrometer. Journal for Advanced Instrumentation in Science (2022). DOI: 10.31526/jais.2022.264.